

TURBULENT TRANSPORT IN ISOLATED TRAILING VORTICES

Karthik Duraisamy

Department of Aerospace Engineering,
University of Glasgow, Glasgow, Scotland
dkarthik@eng.gla.ac.uk

Sanjiva K Lele

Department of Aeronautics and Astronautics and Mechanical Engineering,
Stanford University, Palo Alto, CA, USA.
lele@stanford.edu

ABSTRACT

In this work, the temporal evolution of a low swirl-number turbulent Batchelor vortex is studied using direct numerical simulations. The physics of the evolution is investigated with an emphasis on the various mechanisms that influence the transport of axial and angular momentum. Two new conserved quantities are derived and these prove to be useful in achieving a better understanding of the transport process. The formation and evolution of structures that generate mean counter-signed axial and azimuthal vorticity (in an opposite sense to the initial vorticity) appears to play a key role in momentum transport. The characteristics, generation and evolution of the Reynolds stresses is also addressed.

INTRODUCTION

The turbulent Batchelor vortex is representative of practical tip vortices trailed from airplane wings and helicopter rotors. This flow is characterized by mean axial and azimuthal vorticity distributions given by qe^{-r^2} and re^{-r^2} , respectively. The swirl number q thus sets the relative magnitudes of the axial and azimuthal velocities. It is well known (for instance, Ref. [1]) that when the axial shear is strong enough ($q < 1.5$), the flow is linearly unstable to helical normal mode perturbations of a certain shape. Although other types of instabilities [2] exist, the above instability is known to be particularly strong, as has been observed from non-linear [3] and turbulent [4, 5] evolution of this flow. In the unstable range, inviscid-driven helical normal-mode instabilities are seen to grow, but the non-linear interactions with the mean flow result in a saturation (during which the axial velocity has diminished significantly) and eventual decay. The broad objective of this study is to enhance the present understanding of the evolution process and to obtain physical insight into the mechanisms of turbulent transport of axial and angular momentum.

METHODOLOGY AND PROBLEM SET UP

The vorticity form of the incompressible Navier Stokes equations is solved using a pseudo-spectral approach. A novel way of handling the boundary conditions in such an approach was proposed in [6] and has been previously used for a similar application in [5]. This method can be used for flows in which the vorticity is compact in the two unbounded dimensions and the third direction is periodic. In essence, the velocity in the potential region of the flow is treated analytically (to arbitrary order of accuracy) using a matching procedure. In addition to accurately representing

the boundary conditions (use of periodic boundary conditions in the cross-stream directions can render the vortex centrifugally unstable), this method proves to be highly efficient, since the boundaries of the computational domain can be relatively close to the region of interest.

The initial base flow condition is given by:

$$v_\theta = \frac{v_o\sqrt{\alpha}}{r} \left(1 - e^{-\alpha r^2}\right), \quad v_x = \frac{v_o}{q} e^{-\alpha r^2}, \quad (1)$$

where, $q = 0.5$ (highly unstable configuration) and $v_o, 1/\sqrt{\alpha}$ are reference velocity and length scales, respectively. The Lamb's constant $\alpha = 1.25643$, such that the initial core-radius (identified as the radial location of peak v_θ) is $r_{co} = 1$. For all the plots, time is non-dimensionalized by the 'turnover time' $T = 2\pi v_o/r_{co}$. An isotropic turbulence field made compact in the cross-stream directions by multiplying by a Gaussian function was added to the base flow on maturation. The Reynolds number (defined as $\Gamma/\nu = 2\pi v_o/\sqrt{\alpha}/\nu$) was set at 8000. A domain of size 40×15^2 was discretized on a mesh of dimension 512×192^2 . Runs with varying turbulence intensities and spectral content were performed and it was established that the qualitative features of the evolution remained the same as long as the initial intensity of the turbulence kinetic energy was less than roughly 2% of the mean flow KE. In this paper, a representative run of intensity 0.001% will be analyzed. This will be referred to as Case I (Isotropic). To obtain a better qualitative understanding of various aspects of the evolution, a calculation, termed Case E (Eigenfunction) starting from the most unstable Eigenfunction (from linear normal mode theory) will also be utilized. Case E is initialized at a similar intensity as Case I and is a helically symmetric flow.

EVOLUTION

The temporal evolution of certain global quantities for Case I is shown in fig. 1. From the KE plots, a growth phase, a saturation phase and a decay phase are evident. Spectral analysis revealed that most of the energy during the growth phase was concentrated in the most unstable normal mode (axial wavenumber ≈ 1 and azimuthal wave number ≈ -2), a fact that was also confirmed by flow visualization. For case E, the initial linear growth rate was found to precisely match the results of the normal mode stability analysis. As has been observed previously [3, 4, 5], the peak axial velocity (and hence, the azimuthal vorticity) decays more rapidly than the peak azimuthal velocity (refer fig. 1b, in which all the quantities are normalized by the value at $t=0$), resulting in a more stable configuration (or a higher q) at later times. Figure 1c shows that the core radius (radial location of peak

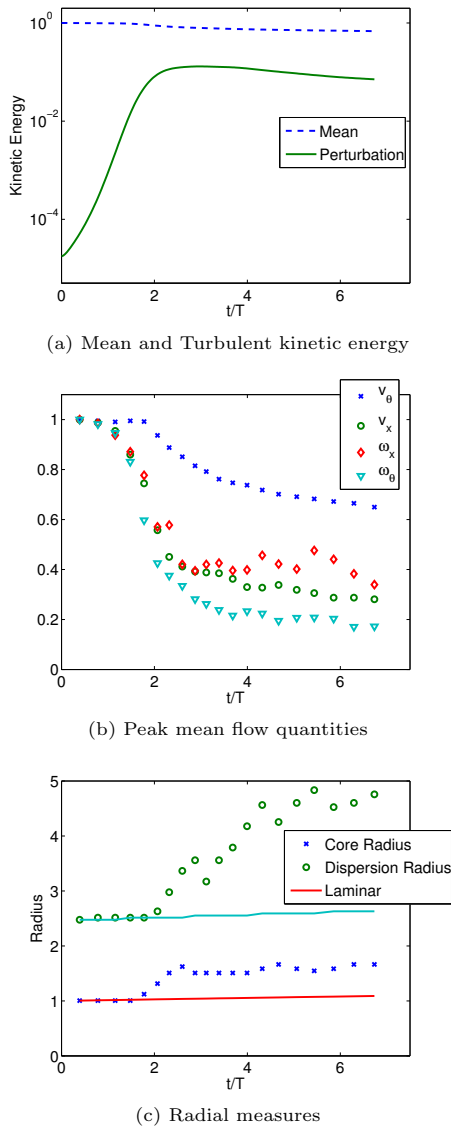


Figure 1: Evolution of global quantities for Case I

tangential velocity) rapidly increases during the saturation phase. As will be seen later, this corresponds to a major change in core structure. Also shown is the ‘Dispersion radius’, which is qualitatively the edge of the turbulent region, and quantitatively defined as the maximum radius at which the mean vorticity is at least 0.5% of the peak vorticity. This is an important measure of the extent of momentum transfer and is seen to grow rapidly even during the decay phase.

Figure 2 shows part of the instantaneous flow-field at the beginning of the decay phase. From the axial and azimuthal vorticity plots (figs. 2b,d), the dominant helical structures inside the core can be seen. Outside the core, vorticity is highly filamented. However, ω_x is still predominantly aligned with the structures inside the core, while ω_θ is primarily aligned in the azimuthal direction. From the mean vorticity plots (fig. 6), it is evident that the outermost ω_x structures are generally of a negative sense, whereas, the corresponding ω_θ structures appear to be of a positive sense. These features are seen throughout the decay process, and their origins can be better understood if Case E is considered (figs. 3,4) and as will be explained later, are also dynamically necessary.

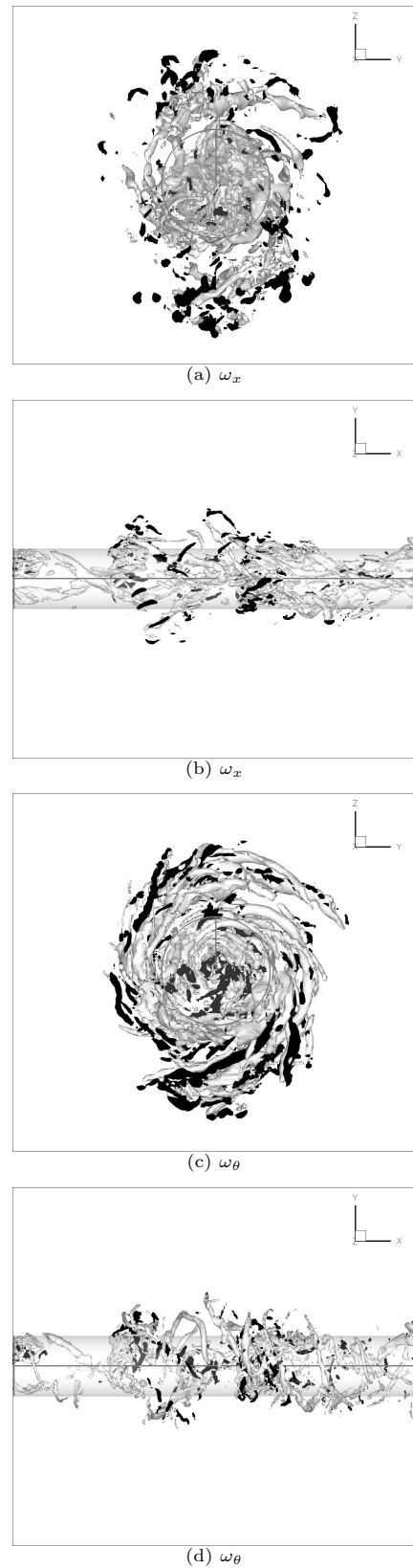
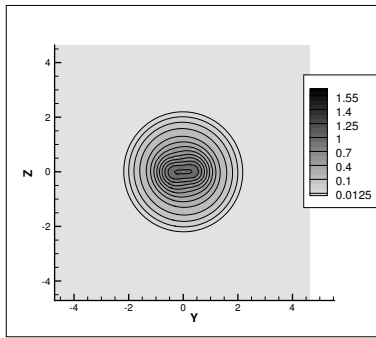
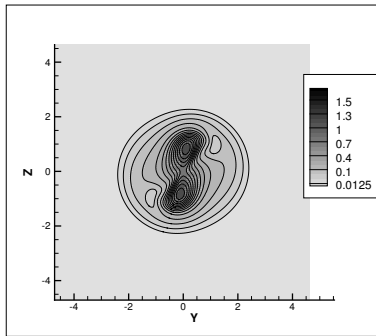


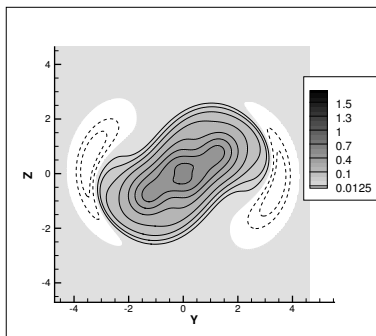
Figure 2: Axial and azimuthal vorticity iso-surfaces for Case I at $t/T = 3.4$. Light surface: $+0.65$, Dark surface: -0.65 . Also shown is a cylinder of radius 1.5



(a) Linear growth



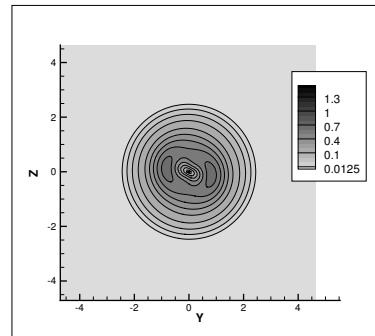
(b) Saturation



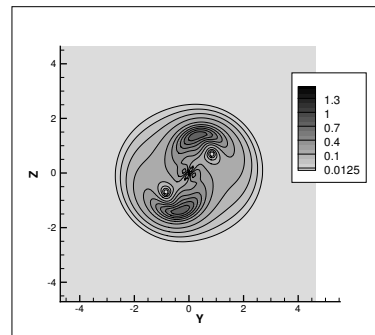
(c) Decay

Figure 3: Axial vorticity contours for Case E. Negative vorticity shown in dashed lines/white patch

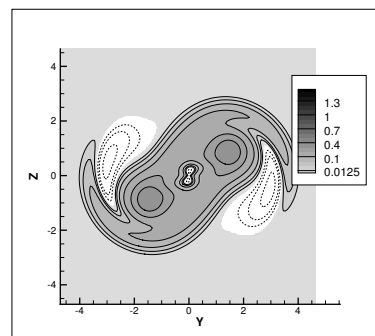
In Case E, as the helical instability (an azimuthal ‘2’ mode) grows, the alternating positive and negative ‘lobes’ of perturbation axial vorticity induce a radial velocity field that tends to disturb the mean axial vorticity. Initially, the vorticity near the axis is distorted elliptically, with the major axis aligned with the positive perturbation lobes. Subsequently, the stretching of the major axis of the ellipse results in a migration of the mean vorticity toward the positive lobes. This linear growth is maintained until a point when enough vorticity has migrated toward the positive perturbation lobes (at this instant the vortex tubes enclosing the axis form small localized grooves, implying significant radial vorticity), that the symmetry of the perturbations is lost due to non-linear interactions with the mean flow. (Figure 3b shows a representative instant, at which the ‘2’ mode symmetry is clearly lost). The orientation of the total vorticity is such that the negative perturbation lobes are distorted and drawn toward the center of the positive lobes. The migration of the negative perturbation lobes to a larger radius (fig. 5) results in the generation of mean negative axial and azimuthal vorticity at the edge of the core since the mean



(a) Linear growth



(b) Saturation



(c) Decay

Figure 4: Azimuthal vorticity contours for Case E. Negative vorticity shown in dashed lines/white patch

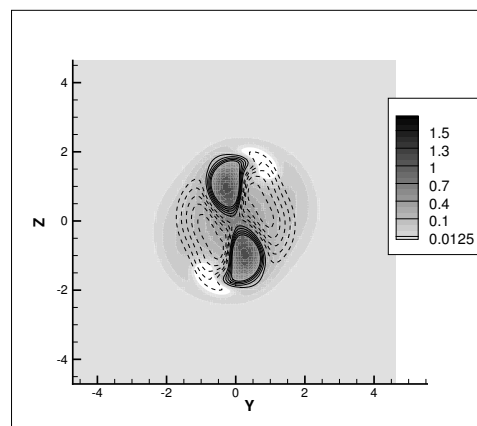


Figure 5: Case E (Saturation): Axial vorticity contours (shaded) superimposed with perturbation axial vorticity contours (lines). Negative vorticity shown in dashed lines/white patch

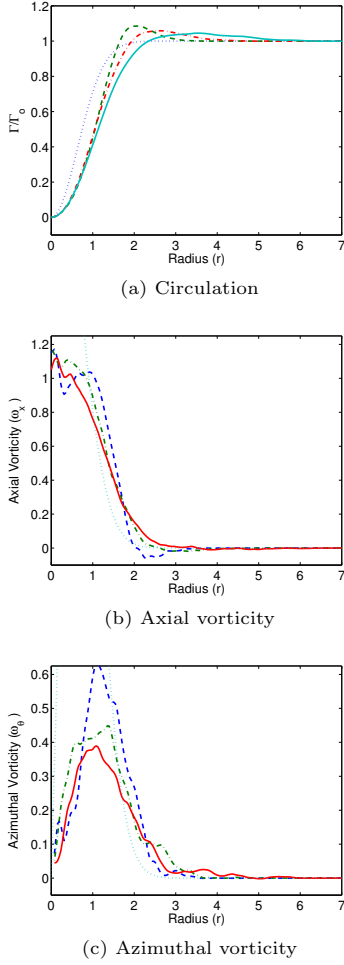


Figure 6: Evolution of mean quantities for Case I. Dashes: $t/T = 2.6$, Dash-Dot: $t/T = 3.4$, Solid: $t/T = 5$. Initial condition also shown

vorticity was originally small at these locations. (figs. 3c and 4c - beginnings of the negative axial vorticity generation can be seen in fig. 3b at $\{\pm 1.5, \pm 1\}$) These structures continue to move radially outward along with a helical annulus of opposite (positive) sense (at a smaller radius for ω_x and a larger radius for ω_θ). The convection of these structures is significant for momentum transport in the radial direction and their presence can be seen in both cases ($r > 2$ in fig. 6, fig. 7). The presence of the mean negative ω_x near the edge of the core corresponds to a circulation overshoot (fig. 6a). The presence of a local positive peak of ω_θ , while exaggerated in fig. 7b can also be seen in fig. 6c. In the following section, the presence of these structures will be explained from dynamic considerations. At the latest investigated time for Case E, similar to the findings in [3], the negative vortical structures are convected away from the core and an apparently stable system composed of two helical lobes is observed. In Case I however, the breakdown of the dominant helical structures appear to drive the system toward a stable high- q Batchelor vortex configuration.

CONSERVED QUANTITIES

It is well known [4] that the integral relations for angular and axial momentum for mean axisymmetric flow (homoge-

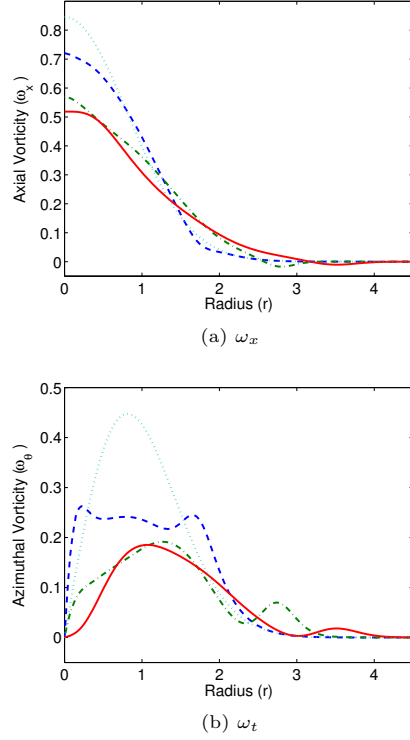


Figure 7: Evolution for Case E during the decay phase. Dashed line is earliest shown instant and Solid line is latest. Laminar solution corresponding to earliest instant also shown

neous in the axial direction) are given by

$$\frac{\partial}{\partial t} \left[\int_0^R r^2 v_\theta dr \right] = -[r^2 \overline{v'_r v'_\theta}]_{r=R} - \nu \frac{\Gamma_o}{\pi}, \quad \text{and}, \quad (2)$$

$$\frac{\partial}{\partial t} \left[\int_0^R r v_x dr \right] = -[r \overline{v'_r v'_x}]_{r=R} \quad (3)$$

In the present computations, it was confirmed that $\overline{r^2 v'_r v'_\theta}$ and $\overline{r v'_r v'_x}$ were both very small at large radii, and hence, total axial momentum is conserved and the total angular momentum depends only on the viscosity (and decays very slowly at large Reynolds numbers).

Presently, decomposing the instantaneous velocity field into a laminar solution (denoted by subscript l) at that instant and a ‘ δ ’,

$$\{U, V, W\}(x, r, \theta, t) = \{v_{x,l}, 0, v_{\theta,l}\}(r, t) + \{u, v, w\}(x, r, \theta, t), \quad (4)$$

the following new relations were derived:

$$\frac{\partial}{\partial t} \left[\int_0^R \widetilde{r^2 w} dr \right] = \left[-r^2 \widetilde{w} + \nu r^3 \frac{\partial}{\partial r} \left(\frac{w}{r} \right) \right]_{r=R} \quad (5)$$

and,

$$\frac{\partial}{\partial t} \left[\int_0^R \widetilde{ur} dr \right] = \left[-r \widetilde{u} + \nu r \frac{\partial u}{\partial r} \right]_{r=R}, \quad (6)$$

where, $\widetilde{a} = \int_0^{2\pi} a d\theta$. It was confirmed that the right hand sides of the above equations were indeed zero, and therefore, the ‘ δ ’ angular and axial momentum flux are conserved, and do not appear to depend on the viscosity. These relations are significant because they can be used to study the transport

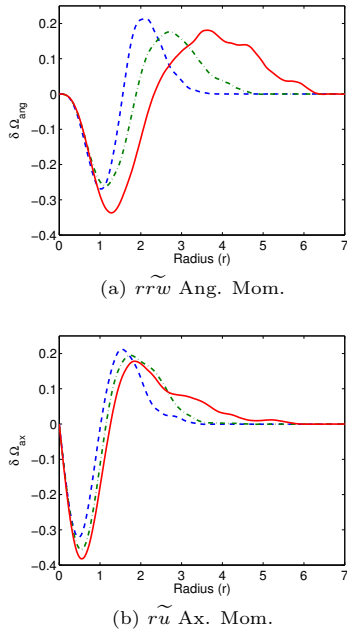


Figure 8: Evolution of ‘ δ ’ quantities for Case I. Dashes: $t/T = 2.6$, Dash-Dot: $t/T = 3.4$, Solid: $t/T = 5$

of momentum within the vortex flow field. Figure 8 shows the evolution of the afore mentioned quantities (more specifically, the LHS integrands) during the decay process. Clearly, there is a net loss of momentum (compared to the laminar evolution) inside the core and this is transferred to the exterior. It has to be recognized that the turbulent transport of mean angular and axial momentum is solely dependent on the terms $-\frac{\partial}{\partial r} r^2 \widetilde{v_r'v_\theta'}$ and $-\frac{\partial}{\partial r} r \widetilde{v_r'v_x'}$, respectively.

The ‘ δ ’ angular momentum can be expressed as

$$\widetilde{r^2 w}(r) = r \int_0^r \omega_x - \omega_{x,l} r dr, \quad (7)$$

Then if $\widetilde{\omega_x}(r) > \omega_{x,l}(r) + \epsilon_x$ (a very plausible situation considering the fact that mean ω_x has convected to a larger radii from the axis) at some $r = r_1$, then, $\widetilde{\omega_x}(r) < \omega_{x,l}(r)$ at some $r = r_2 > r_1$. ($\epsilon_x > 0$ is related to the initial perturbation angular momentum). This is because the net ‘ δ ’ angular momentum has to be conserved and also due to the consistency condition at $r = 0$ as well as the compactness of \widetilde{w} . Evidence of this can be seen from fig. 7a, in which, at the earliest shown instant, a sudden drop in ω_x (to a value below $\omega_{x,l}$) is observed near the edge of the vortical region. At later instances, the corresponding $\omega_{x,l} = 0$ (because laminar diffusion is much slower) and hence $\omega_x = -\partial/\partial r v_x$ has to drop to negative levels to satisfy conservation.

Similarly, conservation of axial momentum flux implies that if $v_x(r) < v_{x,l}(r) - \epsilon_\theta$ (again, a possible situation because axial velocity decays at a higher rate than the laminar case) at some $r = r_1$, then, $v_x(r) > v_{x,l}(r)$ at some $r = r_2 > r_1$. During the decay phase, in comparison to the laminar case, since the peak axial velocity in the core is likely to be at smaller levels and the core radius is larger, the deficient momentum is likely to be regained outside the core. The requirement for compactness then assures $v_x = 0$ at some radius, resulting in a positive ω_θ . This can be seen in fig. 6c and fig. 7b.

REYNOLDS STRESS EVOLUTION

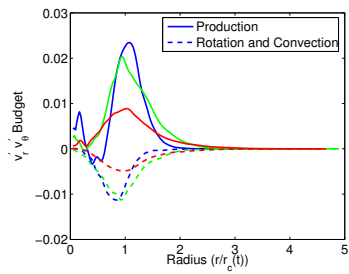
During the linear growth stage, all the components of the Reynolds stress are concentrated in annuli, primarily inside the core. $\overline{v_r'^2}$ and $\overline{v_x'^2}$ peak at $0.6r_c(t)$ while $\overline{v_\theta'^2}$ peaks around $0.3r_c(t)$. Similar observations have been previously reported for a vortex with $q = 1.0$ in [4], in which a detailed analysis of the Reynolds stress budgets is also presented. During saturation and decay, these peaks move toward the vortex axis. As has been observed experimentally [7] and computationally [4], $\overline{v_r'^2} > \overline{v_\theta'^2}$ because the primary production terms are of opposite sign. While the respective production terms of the Reynolds normal stresses peak away from the axis and dominate during the growth phase, the pressure (strain and transport) and the turbulent transport terms appear to be more significant during saturation and decay and are more active near the vortex axis. As a result, the normal stresses are concentrated near the axis during decay. In the potential part of the flow, the relation $\overline{v_x'^2} = \overline{v_r'^2} + \overline{v_\theta'^2}$ is approximately satisfied.

The primary Reynolds shear stress components, $\overline{v_r'v_\theta'}$ and $\overline{v_x'v_r'}$ initially peak around a radius $0.6r_c(t)$, but continue to migrate in a radially outward direction. The respective production terms in the Reynolds stress transport equations are: $P_{r\theta} = -s_{r\theta}(\overline{v_r'^2} + \overline{v_\theta'^2})$ and $P_{xr} = \omega_\theta(\overline{v_x'^2} + \overline{v_r'^2})/2$. (Note: $-s_{r\theta} = -(\partial v_\theta/\partial r - v_\theta/r)/2$ and ω_θ are primarily positive. Also, the above terms represent only the ‘significant’ part of the production terms.) During the growth phase, the production terms are clearly dominant and dependent on the Reynolds normal stresses. During the decay phase as seen in fig. 9a, $P_{r\theta}$ decays rapidly inside the core and relatively slowly outside it (in fact, there is even some growth). It was also confirmed that the turbulent transport and pressure terms were not significant outside the core. Therefore, the peak $\overline{v_r'v_\theta'}$ migrates outside the core (fig. 9c). This means that angular momentum is efficiently transported radially outward.

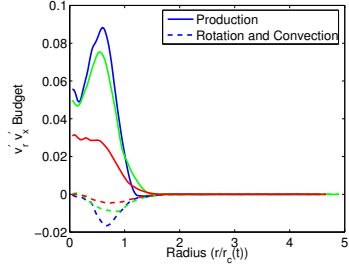
In contrast to $P_{r\theta}$, P_{xr} is primarily concentrated inside the core. This is because the former depends on the mean strain rate (which extends to $r \rightarrow \infty$), whereas the latter depends on the vorticity (which is mainly concentrated within $r < r_c(t)$). Accordingly, while the budget of $\overline{v_r'v_\theta'}$ outside the core is dominated by the production terms, the radial outward spread of $\overline{v_x'v_r'}$ is additionally dictated by the pressure and turbulent transport terms. Since the vorticity and Reynolds normal stresses are significant inside the core, P_{xr} is dominant inside the core, and hence, there is some generation of $\overline{v_x'v_r'}$ near the axis. It was also observed that, in general, the contribution of the turbulent transport terms is larger in the Reynolds normal stress budgets than in the shear stress budgets.

GENERATION OF $\overline{V_R'V_\theta'}$

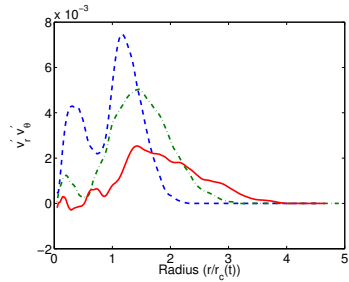
As mentioned earlier, efficient transport of angular momentum is governed by the generation and transport of $\overline{v_r'v_\theta'}$. In this section, the associated physical mechanisms are sought for. For a qualitative picture, consider fig. 10a. The prominent vortical features are the two positive ω_x and the two negative ω_x structures. If only the positive ω_x structures were present, four $\overline{v_r'v_\theta'}$ lobes (around each ω_x structure) of alternating sign will be generated. The presence of the additional negative ω_x structures results in an induced velocity field that generates positive $\overline{v_r'v_\theta'}$, mainly outside the core. A similar mechanism appears to be in play in Case I (fig. 10b), where toward the bottom left corner, the presence of structures surrounding the mean positive ω_x generate a lo-



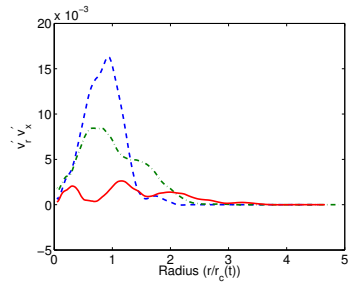
(a) Budget for $\overline{v'_r v'_\theta}$



(b) Budget for $\overline{v'_x v'_r}$



(c) $\overline{v'_r v'_\theta}$



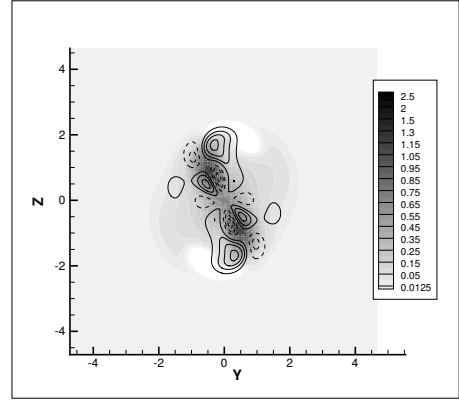
(d) $\overline{v'_x v'_r}$

Figure 9: Reynolds stress and some budgets for Case I at times $t/T = \{2.6, 3.4, 5\}$, with increasing time corresponding to decreasing peak production

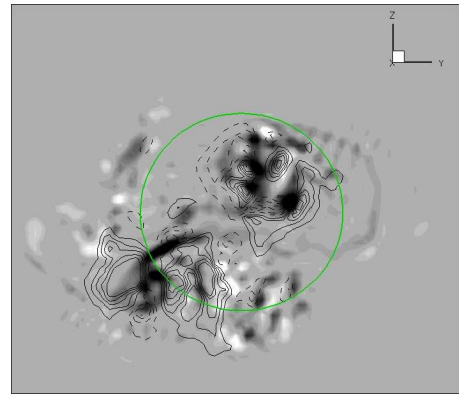
cal positive correlation of $v'_r v'_\theta$. Also note that the presence of a secondary counter-rotating structure will result in an additional strain-rate, thus strengthening $P_{r\theta}$.

SUMMARY

A range of issues related to the temporal evolution of an initially unstable turbulent Batchelor vortex were addressed. Considerable qualitative insight on the flow was obtained by studying the non linear evolution of a single instability mode. The deviation of the mean angular and axial momentum from the laminar solution was shown to be conserved and this was seen to dictate the existence and evolution of mean counter-signed vorticity. Physical insight was provided on



(a) Case E, Saturation phase



(b) Case I, $t/T = 3.4$

Figure 10: Representative instantaneous streamwise sections during the decay phase. Contours of ω_x and lines of $v'_r v'_\theta$ shown. Negative ω_x shaded dark, Negative $v'_r v'_\theta$ shown in dashed lines

the generation and evolution of these structures and their role in the radial transport of momentum.

*

References

- [1] Fabre, D. & Jacquin, L., 2004, "Viscous instabilities in trailing vortices at large swirl numbers," *Journal of Fluid Mechanics*, **500**.
- [2] Heaton, C. & Peake, N. 2006, "Algebraic and exponential instability of inviscid swirling flow," *Journal of Fluid Mechanics*, **565**.
- [3] Delbende, I. & Rossi, M., 2005, "Nonlinear evolution of a swirling jet instability," *Physics of Fluids*, **17**.
- [4] Qin, J., 1998, "Numerical simulations of a turbulent axial vortex," *Ph.D. Dissertation*, Purdue University.
- [5] Duraisamy, K., and Lele, S., 2006, "DNS of temporal evolution of isolated turbulent vortices," *Proc. 2006 CTR Summer Program*, Stanford University.
- [6] Rennich, S. & Lele, S., 1997, "Numerical method for incompressible vortical flows with two unbounded directions," *Journal of Computational Physics*, **137** (1).
- [7] Chow, J.S., Zilliac, G.G. & Bradshaw, P., 1997, "Mean and turbulence measurements in the near field of a wingtip vortex," *AIAA Journal*, **35** (10).